

Beam-helicity asymmetry in photon and pion electroproduction in the $\Delta(1232)$ resonance region at $Q^2 = 0.35$ (GeV/c) 2

I.K. Bensafa¹, P. Achenbach², M. Ases Antelo², C. Ayerbe², D. Baumann², R. Böhm², D. Bosnar⁵, E. Burtin³, X. Defay¹, N. D'Hose³, M. Ding², M.O. Distler², L. Doria², H. Fonvieille^{1,a}, J.M. Friedrich⁸, J. Friedrich², J. García Llongo², P. Janssens⁴, G. Jover Mañas², M. Kohl², G. Laveissière¹, M. Lloyd², M. Makek⁵, J. Marroncle³, H. Merkei², P. Merle², U. Müller², L. Nungesser², B. Pasquini⁷, R. Pérez Benito², J. Pochodzalla², M. Potokar⁶, G. Rosner⁹, S. Sánchez Majos², M. Seimetz^{2,3}, S. Širca⁶, T. Spitzenberg², G. Tamas², R. Van de Vyver⁴, L. Van Hoorebeke⁴, Th. Walcher², and M. Weis²

¹ Laboratoire de Physique Corpusculaire IN2P3-CNRS, Université Blaise Pascal, F-63170 Aubière Cedex, France.

² Institut für Kernphysik, Johannes Gutenberg-Universität, D-55099 Mainz, Germany.

³ CEA Dapnia-SPhN, C.E. Saclay, F-91191 Gif-sur-Yvette Cedex, France.

⁴ Department of Subatomic and Radiation Physics, University of Gent, B-9000 Gent, Belgium.

⁵ Department of Physics, University of Zagreb, HR-10002 Zagreb, Croatia.

⁶ Institut Jožef Stefan, University of Ljubljana, SI-1001 Ljubljana, Slovenia.

⁷ Dipartimento di Fisica Nucleare e Teorica, Università degli Studi di Pavia, and INFN, Sezione di Pavia, Pavia, Italy.

⁸ Physik Department, Technische Universität München, D-85748 Garching, Germany.

⁹ Department of Physics and Astronomy, University of Glasgow, Glasgow G12 8QQ, UK.

Received: date / Revised version: date

Abstract. The beam-helicity asymmetry has been measured simultaneously for the reactions $\vec{e} p \rightarrow e p \gamma$

and $\vec{e} p \rightarrow e p \pi^0$ in the $\Delta(1232)$ resonance region at $Q^2 = 0.35$ (GeV/c) 2 . The experiment was performed at MAMI with a longitudinally polarized beam and an out-of-plane detection of the proton. The results are compared with calculations based on Dispersion Relations for virtual Compton scattering and with the MAID model for pion electroproduction. There is an overall good agreement between experiment and theoretical calculations. The remaining discrepancies may be ascribed to an imperfect parametrization of some $\gamma^{(*)} N \rightarrow \pi N$ multipoles, mainly contributing to the non-resonant background. The beam-helicity asymmetry in both channels (γ and π^0) shows a good sensitivity to these multipoles and should allow future improvement in their parametrization.

PACS. 13.40.-f Electromagnetic processes and properties – 13.60.Fz Elastic and Compton scattering – 13.60.Le Meson production – 14.20.Gk Baryon resonances with S=0

1 Introduction

Polarization observables are powerful tools to study hadron structure. They have seen intensive developments in the recent years in semi-inclusive and exclusive reactions, at high and low energies. At high energies they are detailed probes of mechanisms at the parton level, e.g. in the study of the transverse spin structure of the nucleon in semi-inclusive deep inelastic scattering [1], or of the generalized parton distributions in exclusive deep virtual Compton scattering (DVCS) [2]. At lower energies, models of nucleon structure have to address the non-perturbative regime of QCD without the help of hard sub-mechanisms. The relevant degrees of freedom can be quarks, like in constituent quark models, or bare hadrons surrounded by a

pion cloud, like in chiral perturbation theories. Polarization observables provide specific insights, since they are more sensitive to different amplitude combinations, or interferences, than unpolarized cross sections. For example an important effort is being pursued to investigate the multipoles contributing to the formation of the P_{33} resonance $\Delta(1232)$ by performing low-energy pion electroproduction experiments [3,4].

Photon electroproduction on the proton, $ep \rightarrow ep\gamma$, is another interesting channel for that purpose. It gives access to virtual Compton scattering (VCS) $\gamma^* p \rightarrow \gamma p$. This process has a sensitivity to the electromagnetic structure of the nucleon that is complementary to that of, e.g., elastic scattering or pion production. At low energy W in the (γp) center-of-mass system, the VCS process allows to access the generalized polarizabilities (GPs) of the nucleon, related to the VCS amplitude at vanishing en-

^a corresponding author, e-mail helene@clermont.in2p3.fr

ergy of the outgoing photon [5]. These observables have been measured recently at different values of the four-momentum transfer squared Q^2 at MAMI [6], JLab [7] and MIT-Bates [8].

When going above the pion threshold, the VCS amplitude T^{VCS} acquires an imaginary part due to the coupling to the πN channel. Therefore single polarization observables, which are proportional to $\text{Im}(T^{VCS})$, become non-zero above pion threshold. A particularly relevant observable is the beam-helicity asymmetry (SSA): $SSA = (\sigma^\uparrow - \sigma^\downarrow)/(\sigma^\uparrow + \sigma^\downarrow)$ where σ^\uparrow and σ^\downarrow designate the photon electroproduction cross section with beam helicity state + and -, respectively. As it was first pointed out in ref. [9], the SSA yields direct information on the absorptive part of the VCS amplitude, and on the relative phase between the VCS amplitude and the Bethe-Heitler (BH) contribution. The BH process refers to the photon emission by the incoming or outgoing electron and it adds coherently to the VCS amplitude. Moreover, the VCS amplitude can be split into a Born part, given in terms of nucleon ground state properties (the electromagnetic form factors), and a non-Born part which contains all nucleon excitations and meson-loop contributions. Since the BH and Born-VCS contributions are purely real, the SSA is proportional to the imaginary part of the non-Born VCS amplitude. In particular, the numerator of the SSA can be written as $\text{Im}(T^{VCS}) \cdot \mathcal{R}(T^{VCS} + T^{BH})$. After development, one obtains the sum of a pure VCS contribution and a VCS-BH interference term which has the effect to enhance the asymmetry. The absorptive part of the VCS amplitude can be obtained, through unitarity relation, from the photo- and electro-production amplitudes on the nucleon. In the region of $W \sim 1.2$ GeV, the most important contribution is from πN intermediate states, as schematically depicted in fig. 1, while mechanisms involving more pions or heavier mesons in the intermediate states are suppressed. Regarding the Q^2 -dependence, the pion photoproduction description is on solid experimental grounds, while electro-production data are scarce. Therefore a measurement of the beam SSA in the Δ -resonance region gives a direct test of how well the description of the VCS amplitude holds, in terms of the available phenomenological information on pion photo- and electro-production amplitudes. This is the main purpose of the experiment described in the present paper.

In the case of DVCS one has a known ϕ -dependence of the numerator and denominator of the SSA. In our kinematic regime this dependence is not known analytically. However, the Dispersion Relations (DR) model calculation discussed in section 4 gives a shape of the asymmetry close to a $\sin \phi$, despite the distortion of the numerator and denominator due to the BH process.

Since in the experiment the reaction $ep \rightarrow ep\pi^0$ was detected too, the beam SSA was also measured in this channel, complementing previous measurements of this type at different kinematics [3]. In pion electroproduction, the beam SSA, also called ρ'_{LT} , is proportional to the fifth structure function R'_{LT} [10] and is mainly sensitive to the

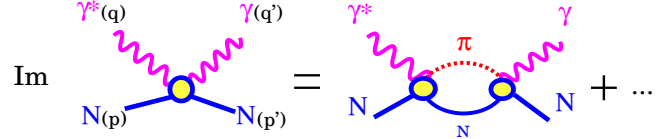


Fig. 1. The imaginary part of the VCS amplitude decomposed using unitarity.

Table 1. Experimental settings for spectrometers A (electron arm) and B (proton arm): values of the horizontal angles θ_A and θ_B w.r.t. the beam direction, and the central momenta p_A and p_B . α_{oop} is the out-of-plane angle of spectrometer B.

θ_A	p_A (MeV/c)	θ_B	p_B (MeV/c)	α_{oop}	setting
59.9°	401.2	25.2°	345	2°	OOP-1
		20.3°	358	7°	OOP-2
		15.0°	398	10°	OOP-3

multipole ratios S_{1+}/M_{1+} and S_{0+}/M_{1+} in the region of the Δ resonance.

2 The experiment

The experiment was performed at the Mainz Microtron MAMI using the 100 % duty cycle electron beam at an energy of 883.2 MeV, allowing for a longitudinal beam polarization P_e of 75-85 %. Helicity reversal was performed every second, and beam current values were typically 13-25 μA . The experiment used the standard equipment of the A1 collaboration [11]: the Möller polarimeter to measure P_e once a day, the 5 cm long liquid Hydrogen target, spectrometer A to detect the scattered electron at a fixed setting, and spectrometer B to detect the final proton at three different out-of-plane settings. Table 1 summarizes the kinematical settings, corresponding to an average Q^2 of 0.35 (GeV/c)² and a virtual photon momentum in the center-of-mass $q_{cm} = 600$ MeV/c, similar to a previous VCS experiment at MAMI [6]. However, here W is above pion threshold ($W \sim 1.2$ GeV) and the virtual photon polarization $\epsilon = 0.48$ is the highest achievable at this value of W .

The detector package in each spectrometer includes a set of two double-planes of vertical drift chambers (VDC) for particle tracking and two segmented planes of scintillators for particle identification and timing measurements. The experiment also uses the threshold gas Čerenkov counter in spectrometer A for electron identification. The beam was off-centered horizontally in order to minimize the path-length in Hydrogen for the low-energy emitted protons. Analysis cuts include particle identification for the final electron and proton, good quality tracks in the VDCs, and rejection of backscattered protons at the entrance window of spectrometer B. A specific cut is applied to eliminate protons emitted at the most upward angles, which hit a piece of the target holding system. Empty target cell studies showed that the rate of background events from

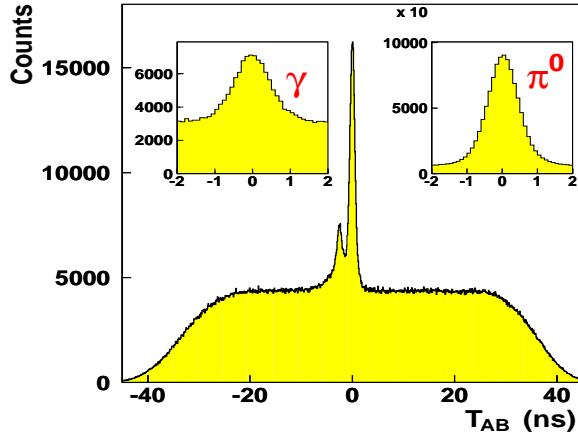


Fig. 2. The coincidence time spectrum for a sample of the data (no cuts). Inserts: zoom on the central peak after analysis cuts, for the full statistics in both channels: γ (left) and π^0 (right) electroproduction.

$eA \rightarrow epX$ reactions in the target walls was negligible compared to the rate of $ep \rightarrow ep\pi^0$ events, but not negligible compared to the rate of $ep \rightarrow e\gamma$ events. Therefore a cut on the target length is applied in the analysis of the γ channel, but not in the π^0 channel.

Fig. 2 shows the spectrum of coincidence time (T_{AB}) for triggers in coincidence between the two spectrometers. The central peak represents the true (e, p) coincidences and has a FWHM of 1 ns. Without any cuts, one notices a secondary peak near $T_{AB} = -2$ ns due to true (π^-, p) coincidences, which is eliminated by a cut on the Čerenkov counter signal in spectrometer A. After all cuts, the level of random coincidences is still high for the γ channel, as illustrated by the insert on fig. 2. Events are selected within ± 1.4 ns in the central peak, and random coincidences are subtracted using side-band events.

The four-momentum of the third, undetected particle is reconstructed by the missing energy and missing momentum associated to the detected (ep) system. Fig. 3 shows the final spectrum of the missing mass squared (M_x^2). The most prominent peak is due to π^0 electroproduction events. The second peak, centered on $M_x^2 = 0$, is due to photon electroproduction events, and its smallness reflects the smallness of the corresponding cross section. This spectrum is obtained after a careful calibration of experimental parameters, such as the beam position along the horizontal transverse axis, a casual layer of frost on the target walls, and the central momentum of spectrometer B for each run period, which was changed by less than a few 10^{-3} w.r.t. its nominal value. The separation between the two peaks in M_x^2 is well-achieved. Both peaks are similar in shape: they have the same central width due to experimental resolution, and a radiative tail extending to larger values. An empirical fit of this shape (see curves on fig. 3) allows to quantitatively estimate the residual π^0 events under the photon peak, yielding a contamination $C = 4\%$. All other background processes, e.g. coming

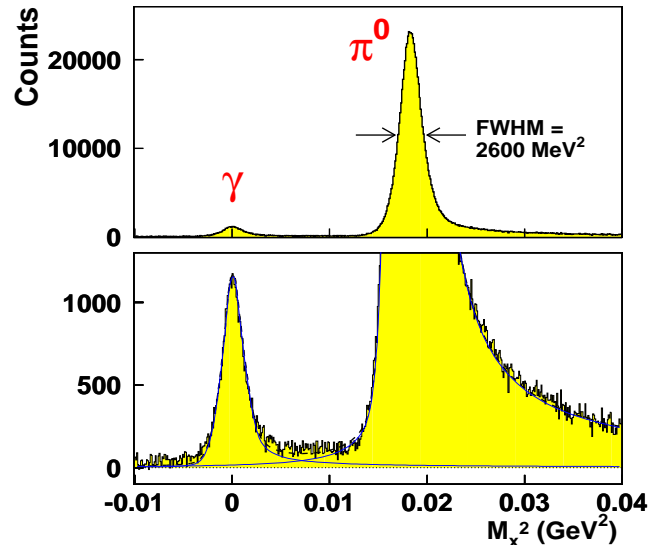


Fig. 3. Top: the missing mass squared spectrum within analysis cuts and after subtraction of random coincidences. Bottom: the same histogram truncated in ordinate to enhance the photon peak, plus a fit function drawn for each peak (solid lines) and the sum (dashed line).

from the target walls, are reduced to a negligible level within the analysis cuts. Finally, the two physics channels are selected by the following cuts in M_x^2 : $[-0.005, 0.005]$ GeV^2 for the $ep \rightarrow e\gamma$ process and $[0.013, 0.029]$ GeV^2 for the $ep \rightarrow ep\pi^0$ process. The achieved statistics are then 38k true γ events and 1M true π^0 events. More details on the analysis can be found in refs. [12,13].

3 Analysis method and results

Fig. 4 shows the angular phase space coverage for photon electroproduction events: $\theta_{\gamma^*\gamma}^{cm}$ is the polar angle between the initial and final photons of the Compton scattering process and ϕ is the azimuthal angle between the leptonic and hadronic planes as illustrated on figure 5. The value of $\phi = +90^\circ$ corresponds to the missing particle emitted along the direction of $\mathbf{k} \times \mathbf{k}'$, where \mathbf{k} and \mathbf{k}' are the momenta of the incoming and scattered electrons. The three settings cover altogether the region of forward polar angles up to 40° , and a domain in ϕ narrowing around 220° as $\theta_{\gamma^*\gamma}^{cm}$ increases.

Since the SSA is a relative quantity, the data do not need to be corrected for detector inefficiencies, deadtimes, etc. Only false asymmetries were checked, and found to be very small: the beam charge asymmetry (for which the data are corrected) is of the order of 10^{-3} . The phase space is binned in $\theta_{\gamma^*\gamma}^{cm}$ (4° wide, large compared to the experimental resolution) and in each θ -bin the SSA is determined as one value, corresponding to one central kinematical point. To this end the asymmetry is fitted to the assumption $SSA = K \cdot \sin \phi$ (cf. section 1) and the factor K is determined by a maximum likelihood method.

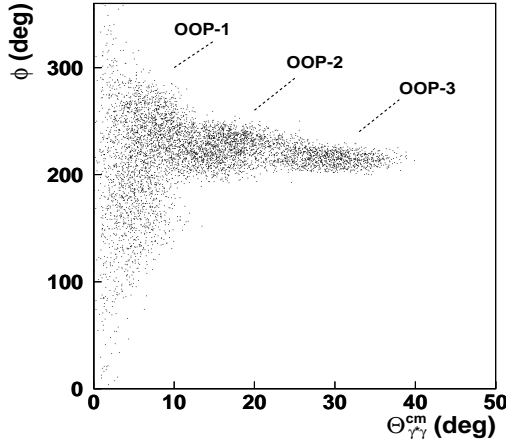


Fig. 4. The accepted phase space in terms of the polar and azimuthal angles of the Compton scattering process.

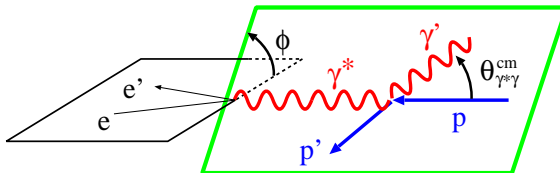


Fig. 5. Kinematics of the $ep \rightarrow ep\gamma$ reaction in the γp center-of-mass.

The probability associated to event i is proportional to $(1 + h_i P_e K \sin \phi_i)$ where h_i is the beam helicity state (+1 or -1) and ϕ_i the azimuthal angle of the event. The likelihood method includes the treatment of random coincidences and also yields the statistical error on K . As a cross-check, a more classical method is used, based on the count rates N^+ and N^- : the asymmetry $A = (N^+ - N^-)/(N^+ + N^-)/P_e$ is calculated in finite bins in ϕ and then fitted to the same shape $A = K \cdot \sin \phi$.

The final asymmetry is computed as $K \cdot \sin 220^\circ$, i.e. it is projected to $\phi = 220^\circ$, a value close to the average over the acceptance. Since the central kinematics vary slightly from bin to bin, one makes a projection to a fixed, nominal kinematics in (Q^2, W, ϵ) :

$$SSA_{nom.kin.}^{exp.} = SSA_{exp.kin.}^{exp.} \times \frac{SSA_{nom.kin.}^{model}}{SSA_{exp.kin.}^{model}}$$

by use of a model: Dispersion Relations [14] for $ep \rightarrow ep\gamma$ and the unitary isobar model MAID [15] for $ep \rightarrow ep\pi^0$. The nominal point corresponds to our average $ep \rightarrow ep\gamma$ kinematics: $Q^2 = 0.35$ (GeV/c) 2 , $W = 1.19$ GeV and $\epsilon = 0.48$. For the π^0 channel, the accepted phase space is very similar. The same analysis method is used, and the asymmetry is projected from the experimental average ($Q^2 = 0.34$ (GeV/c) 2 , $W = 1.21$ GeV, $\epsilon = 0.47$) to the same nominal kinematics as above. This choice results in all projection factors as close as possible to 1, which is desirable in order to minimize projection errors.

Table 2. Summary of systematic errors (more details can be found in [13]).

type of error	amount of error
1) beam polarization	$\Delta P_e/P_e = \pm 0.02$
2) π^0 contamin. (γ)	$\Delta C = \pm 2\%$ ($C = 4\%$)
3) radiative correction	$\pm 100\%$ of the correction
4) proj. to nom.kin.	proj. factor varied by $\pm 10\%$
5) calibration of momenta and angles	$\Delta\theta_A = \pm 0.5$ mrad (electron) $\Delta p_B/p_B = \pm 1 \cdot 10^{-3}$ (proton)
6) stability within cuts	cuts in T_{AB} , acceptance, M_x^2 etc.

Systematic errors are estimated from the sources of uncertainty listed in table 2. These errors are propagated to the asymmetry, either analytically (items 1 to 4) or by running the analysis in different conditions (items 5, 6) and taking the spread of the resulting SSA. Concerning item 2, the SSA in photon electroproduction is corrected for π^0 contamination, using $SSA = SSA_{raw} \cdot (1 + C)$ to first order, and a $\pm 50\%$ uncertainty is applied on C . Concerning item 3, radiative corrections to the asymmetry are generally small, as shown in [16, 17]. They have been computed for the present kinematics [18, 19] and found negligible, therefore they are ignored in the analysis. However, an error is assigned to this procedure; the error considered in table 2, item 3, is a way to account for model uncertainties that are present in the calculation of radiative corrections. Items 1 to 4 of this table yield very small errors; the dominant systematic errors come from items 5 and 6. The main errors of the calibration are in the electron scattering angle and the proton-arm central momentum; other calibration parameters (see section 2) have much less influence. The quadratic sum of partial systematic errors bin-per-bin is presented in table 3 together with our final SSA result and its statistical error. The latter is still by far the dominant error. In the VCS channel, the statistical error is enlarged by a factor ~ 1.8 due to the high level of random coincidences.

4 Discussion

4.1 Photon electroproduction channel

The result of the measurement of $\vec{e} p \rightarrow ep\gamma$ is displayed on fig. 6 together with the calculation of the DR formalism of refs. [14, 20]. This model has been developed for real and virtual Compton scattering at moderate energies up to the $\pi\pi N$ threshold. It is the only model available in the literature that calculates specifically $\text{Im}(T^{VCS})$, and therefore is able to predict the beam SSA. The VCS invariant amplitudes are given by s -channel dispersion integrals, in which the imaginary part is calculated through unitarity, taking into account the contribution from πN

Table 3. Beam SSA result for the two reactions, at nominal kinematics: $Q^2=0.35$ $(\text{GeV}/c)^2$, $W=1.19$ GeV , $\epsilon=0.48$, $\phi=220^\circ$.

$\vec{e} p \rightarrow e p \gamma$ channel			
$\theta_{\gamma^* \gamma}^{cm} (\text{deg})$	SSA	ΔSSA_{stat}	ΔSSA_{syst}
2.6	-0.021	0.026	0.015
6.0	-0.035	0.017	0.006
9.8	-0.032	0.020	0.011
14.0	-0.026	0.030	0.016
17.9	-0.014	0.034	0.020
21.9	-0.121	0.044	0.021
26.1	-0.050	0.046	0.023
29.9	-0.053	0.050	0.034
33.7	-0.004	0.070	0.047

$\vec{e} p \rightarrow e p \pi^0$ channel			
$\theta_{\gamma^* \pi}^{cm} (\text{deg})$	SSA	ΔSSA_{stat}	ΔSSA_{syst}
2.5	0.0016	0.0035	0.0017
5.9	-0.0007	0.0028	0.0011
9.9	-0.0059	0.0033	0.0024
14.0	-0.0064	0.0040	0.0018
17.9	-0.0077	0.0043	0.0021
22.1	-0.0055	0.0053	0.0031
26.2	-0.0033	0.0043	0.0022
30.0	-0.0032	0.0039	0.0016
33.7	-0.0078	0.0049	0.0014
37.4	-0.0205	0.0090	0.0039

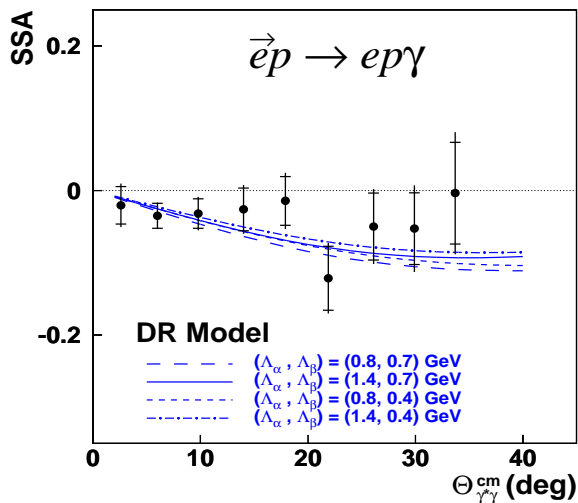


Fig. 6. The beam SSA in photon electroproduction at nominal kinematics compared to the calculation of the DR model (using MAID2003 multipoles) for several values of the free parameters $\Lambda_\alpha, \Lambda_\beta$. The inner error bar is statistical, the outer one is the quadratic sum of statistical and systematic errors.

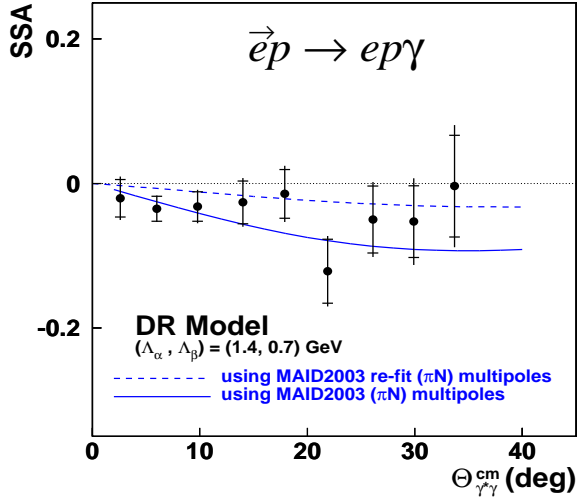


Fig. 7. The beam SSA in photon electroproduction: sensitivity to the MAID (πN) multipoles.

intermediate states. Multipoles for $\gamma^{(*)} N \rightarrow \pi N$ are taken from the MAID 2003 analysis.

The DR model has two free parameters, Λ_α and Λ_β , related to the electric and magnetic GPs and parametrizing their unconstrained part, i.e. asymptotic behaviour and dispersive contribution beyond πN . It is clear from fig. 6 that the SSA exhibits little sensitivity to the GPs. By comparison to the theoretical curves displayed on the figure, one can state that for this given set of πN multipoles the trend of the data is to favor high values of Λ_α and low values of Λ_β , i.e. high values of the electric GP and high values of the magnetic GP.

As explained above, the main feature of the beam SSA is that it is fully sensitive to $\text{Im}(T^{VCS})$. Therefore our measurement is a direct test of the calculation of this quantity. The experimental shape of the SSA in fig. 6 is rather smooth, similarly to the DR prediction. The measured asymmetry is in overall good agreement with the theoretical calculation, although the latter tends to overestimate the magnitude of the asymmetry gradually as $\theta_{\gamma^* \gamma}^{cm}$ increases. This suggests that the calculation of $\text{Im}(T^{VCS})$ can be improved. In that respect, the πN multipoles, which are an essential input to the DR calculation of VCS, may need a better parametrization. It is worth noting that on the one hand the beam SSA in VCS as given by the DR model is insensitive to the change of parametrization from the “2000” to “2003” version of MAID (at least in our kinematics). On the other hand it is sensitive to further “re-fits” such as the one cited in ref. [4], which involves an adjustment of the longitudinal multipoles S_{1+} and S_{0+} in the $\pi^0 p$ channel. In particular, figure 7 shows that the calculation with this re-fit gives a lower asymmetry, in better agreement with the trend of the data at increasing angles. Nevertheless, since this MAID re-fit [4] was performed at kinematics different from the present experiment, there is room left for further

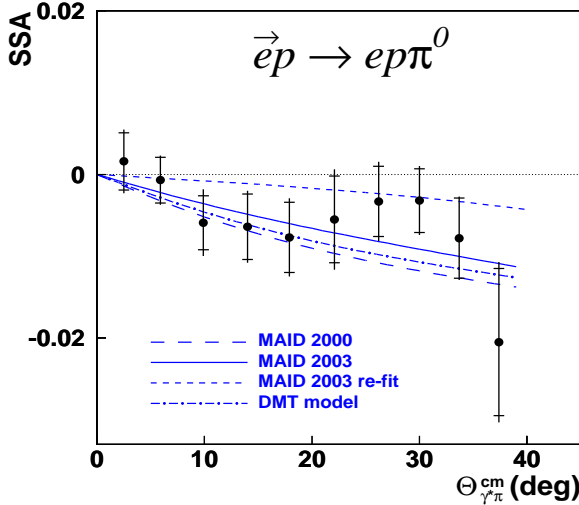


Fig. 8. The beam SSA in π^0 electroproduction at nominal kinematics, compared to theoretical calculations. Same convention as figure 6 for the error bars.

πN multipole adjustment. Other possibilities like contributions beyond πN are very unlikely, since our measured range in W is mostly below the two-pion threshold.

4.2 Pion electroproduction channel

The result of the measurement of $\vec{e} p \rightarrow ep\pi^0$ is displayed on fig. 8. At small angles up to $\theta_{\gamma^*\pi}^{cm} = 20^\circ$, the data are in very good agreement with the MAID model [15] (versions “2000” and “2003”) and the DMT model [21]. Also shown is the MAID re-fit [4] mentioned above, in which the longitudinal multipoles S_{1+} and S_{0+} have been adjusted essentially at $Q^2=0.2$ (GeV/c) 2 . Applied to our Q^2 of 0.35 (GeV/c) 2 [22], this version yields a much lower asymmetry than the other predictions.

Beyond 20° the data of fig. 8 tend to suggest some structure which no model can reproduce. In the s and p wave M_{1+} -dominance approximation, the fifth structure function R'_{LT} is proportional to $\sin\theta_{\gamma^*\pi}^{cm} \cdot \text{Im}\{(6 \cos\theta_{\gamma^*\pi}^{cm} S_{1+} + S_{0+})^* M_{1+}\}$ [10] and so it cannot induce rapid θ -variations of the SSA. To describe such a behavior is quite challenging; it requires the contribution from higher-order multipoles which produce a non-resonant background modulating the resonant M_{1+} contribution.

5 Conclusion

The beam-helicity asymmetry has been measured simultaneously for photon and π^0 electroproduction in the $\Delta(1232)$ resonance region. The measured asymmetries are of the order of a few percent for γ and smaller than 1% for π^0 . There is an overall good agreement between our measurement and the theoretical calculations, based on the DR

and MAID models. The remaining discrepancies in shape or magnitude of the asymmetry might be ascribed to an imperfect parametrization of some πN multipoles, mainly contributing to the non-resonant background.

Concerning virtual Compton scattering, which was the main goal of the experiment, we have performed the first measurement of the beam SSA in photon electroproduction at low energies. The latter provides an important cross-check for the input to the DR formalism for VCS since the imaginary part of the VCS amplitude is connected through unitarity to the $\gamma^{(*)}N \rightarrow \pi N$ multipoles. In order to improve the agreement between experiment and theory for the beam SSA in the photon and electroproduction channels, one could attempt a simultaneous fit of the two observables, by changing the parametrization of some π^0 electroproduction multipoles. In that view, the observables in the two physics channels become coupled. Therefore the data presented in this paper address in a new way important questions by showing how the simultaneous measurements in several de-excitation channels (γN and πN) can help to gain new insights for our understanding of the nucleon and resonance phenomena at low energy.

We thank the MAMI accelerator staff for providing the excellent polarized beam. We thank L.Tiator for valuable discussions and for providing his MAID re-fit result, and M.Vanderhaeghen and G.Smirnov for their contribution to the calculation of radiative corrections. This work was supported by the Deutsche Forschungsgemeinschaft (SFB 443), the Federal State of Rhineland-Palatinate, the French CEA and CNRS/IN2P3, the BOF-Gent University and the FWO-Flanders (Belgium).

References

1. X. Ji et al., Phys. Lett. B638 (2006) 178, hep-ph/0604128.
2. M. Diehl, Phys. Rept. 388 (2003) 41, hep-ph/0307382.
3. P. Bartsch et al., Phys. Rev. Lett. 88 (2002) 142001, nucl-ex/0112009.
4. D. Elsner et al., Eur. Phys. J. A27 (2006) 91, nucl-ex/0507014.
5. P.A.M. Guichon, G.Q. Liu and A.W. Thomas, Nucl. Phys. A591 (1995) 606, nucl-th/9605031.
6. J. Roche et al., Phys. Rev. Lett. 85 (2000) 708.
7. Jefferson Lab Hall A, G. Laveissiere et al., Phys. Rev. Lett. 93 (2004) 122001, hep-ph/0404243.
8. P. Bourgeois et al., Phys. Rev. Lett. 97 (2006) 212001, nucl-ex/0605009.
9. P. Kroll, M. Schurmann and P.A.M. Guichon, Nucl. Phys. A598 (1996) 435, hep-ph/9507298.
10. D. Drechsel and L. Tiator, J. Phys. G18 (1992) 449.
11. K.I. Blomqvist et al., Nucl. Instrum. Meth. A403 (1998) 263.
12. I.K. Bensafa, PhD thesis, UBP Clermont-Ferrand, 2006, DU 1647.
13. H.Fonvieille and I.K.Bensafa, LPC Internal reports PCCF-RI-0604 and PCCF-RI-0605 (2006).
14. B. Pasquini et al., Eur. Phys. J. A11 (2001) 185, hep-ph/0102335.

15. D. Drechsel et al., Nucl. Phys. A645 (1999) 145, nucl-th/9807001, <http://www.kph.uni-mainz.de/MAID/>.
16. M. Vanderhaeghen et al., Phys. Rev. C62 (2000) 025501, hep-ph/0001100.
17. A.V. Afanasev, M.I. Konchatnij and N.P. Merenkov, J. Exp. Theor. Phys. 102 (2006) 220, hep-ph/0507059.
18. H. Fonvieille, LPC Internal report PCCF-RI-0607 (2006).
19. G.I. Smirnov, (2005), hep-ph/0504045.
20. D. Drechsel, B. Pasquini and M. Vanderhaeghen, Phys. Rept. 378 (2003) 99, hep-ph/0212124.
21. S.S. Kamalov and S.N. Yang, Phys. Rev. Lett. 83 (1999) 4494, nucl-th/9904072, <http://www.kph.uni-mainz.de/MAID/dmt/>.
22. L.Tiator, private communication.